*diabetology*

MDPI

*Article*

# Biological Evidence of Improved Wound Healing Using Autologous Micrografts in a Diabetic Animal Model

**Mariza Brandão Palma [1,2,*], Elisa Paolin [3,4], Ismaela Maria Ferreira de Melo [1], Francisco De Assis Leite Souza [1], Álvaro Aguiar Coelho Teixeira [1,2], Leucio Duarte Vieira [5], Fabio Naro [6], Antonio Graziano [4] and Anísio Francisco Soares [1,2]**

1 Department of Morphology and Physiology, Anatomy Unit, Rural Federal University of Pernambuco, Recife 52171-900, Brazil; ismaelamelo@yahoo.com.br (I.M.F.d.M.); francisco.alsouza@ufrpe.br (F.D.A.L.S.); alvaro.teixeira@ufrpe.br (Á.A.C.T.); anisio.soares@ufrpe.br (A.F.S.)
2 Postgraduate Program in Animal Bioscience, Rural Federal University of Pernambuco, Recife 52171-900, Brazil
3 Department of Public Health, Experimental and Forensic Medicine, Human Anatomy Unit, University of Pavia, 27100 Pavia, Italy; elisa.paolin01@universitadipavia.it or elisa.paolin@hbwsrl.com
4 Human Brain Wave, 10128 Turin, Italy; lab@hbwsrl.com
5 Department of Physiology and Pharmacology, Biosciences Center, Federal University of Pernambuco, Recife 50670-901, Brazil; leucio.vieirafo@ufpe.br
6 Department of Anatomical, Histological, Forensic Medicine and Orthopedic Science, Sapienza University of Rome, 00185 Roma, Italy; fabio.naro@uniroma1.it
* Correspondence: mariza.palma@ufrpe.br; Tel.: +55-81-999671506

**Abstract:** Background: Tissue healing consists of four main phases: coagulation, inflammation, proliferation, and remodeling. In diabetic patients, this process is stagnant in the inflammatory stage, leading to chronic wounds. The aim of this study is to evaluate in an animal model the biological evidence related to the use of the Rigenera® technology (Turin Italy), an innovative mechanical procedure to isolate autologous micrografts (AMG). Methods: Fifty male Wistar rats were divided into four groups: control (C), control treated with micrografts (CM), diabetic (DB), and diabetic treated with micrografts (DBM). The experimental setup involved: the quantification of the total collagen and elastic fibers; histopathological analysis; immunohistochemical analysis for collagen type I (COL1), collagen type III (COL3), vascular endothelial growth factor (VEGF-A), and interleukin 4 (IL4) and 10 (IL10); evaluation of the oxidative stress; measurement of gluthatione (GSH); and, finally, an enzyme-linked immunosorbent assay (ELISA) on tumor necrosis factor-α (TNF-α). Results: The AMG technology induces a faster healing process: VEGF-A, IL4, IL10, and GSH increased, while TNF-α and oxidative stress decreased. Conclusions: Animals treated with micrografts showed more favorable results for healing compared to those that did not receive treatment, demonstrating a positive participation of the micrografts in the treatment of difficult-to-heal wounds.

**Keywords:** regenerative medicine; chronic wounds; diabetes; cytokines; skin healing; impaired healing



**Citation:** Brandão Palma, M.; Paolin, E.; Ferreira de Melo, I.M.; De Assis Leite Souza, F.; Coelho Teixeira, Á.A.; Duarte Vieira, L.; Naro, F.; Graziano, A.; Soares, A.F. Biological Evidence of Improved Wound Healing Using Autologous Micrografts in a Diabetic Animal Model. *Diabetology* **2023**, *4*, 294–311. https://doi.org/10.3390/diabetology4030026

Academic Editor: Viorica Patrulea

Received: 6 June 2023
Revised: 7 July 2023
Accepted: 19 July 2023
Published: 28 July 2023



## 1. Introduction

The skin is considered the largest organ in the human body. In an adult, it represents about 16% of the total body weight, and, when distended, it occupies an area of approximately two square meters. Histologically, it is divided into the epidermis, dermis, and hypodermis (also known as the subcutaneous fat layer) [1]. The epidermis is the superficial layer of the skin, and it is composed of keratinized, stratified, and squamous epithelial tissue (Figure 1). It is avascular and receives nutrients by diffusion through the layer just below it, the dermis. In the epidermis, there are distinct layers arranged from the outermost to the innermost region, including the stratum corneum, stratum lucida, stratum granulosum, and stratum spinosum [2]. The deepest layer, known as the basal

layer, is situated adjacent to the dermis, with finger-like projections towards it, referred to as the dermal papillae. The presence of these projections, known as rete ridges, is absent in the early stages of wound healing, which renders the wound more vulnerable to injury if exposed to trauma [3].

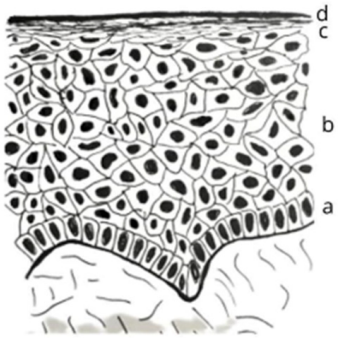


**Figure 1.** Schematic illustration depicting the stratification of the epidermis. The diagram showcases the different layers of the skin, arranged in a hierarchical manner from the deepest to the most superficial regions, namely: (a) the basal layer; (b) the spinous layer; (c) the granular layer; and (d) the stratum corneum. It should be noted that the lucid layer is situated above the granulosa layer, but it is only present in specific areas of the body, such as the tips of the fingers, the soles of the feet, and the palms of the hands.

The basal layer is formed by a single row of cuboidal or columnar keratinocytes, interspersed with stem cells responsible for the renewal of resident cells; it has a great ability to proliferate, and daughter cells migrate towards the skin surface. That suprabasal migration is accompanied by cell maturation until the formation of corneocytes on the skin surface [4]. Their cytoskeleton contains intermediate filaments formed by keratin that attach to desmosomes. In this way, the cells of the basal layer attach to each other and to the adjacent spinous layer [5]. When attached to hemidesmosomes, actin filaments allow the attachment of keratinocytes to the basement membrane, located between the epidermis and the dermis [6].

There are four main types of cells in the epidermis: keratinocytes, melanocytes, Langerhans cells, and Merkel cells. Keratinocytes make up about 90% of the epidermis, and the source of replacement of these cells is the basal layer; they produce the keratin protein that provides protection to the skin and the underlying tissues against heat, chemical agents, and microorganisms [7].

Keratinocytes are identified as the primary cell responsible for the healing of wounds of the epidermis and for maintaining tissue integrity. A stratified keratinized epithelium undergoes constant turnover, regenerating completely in 48 h. Keratinocytes originating from the basal layer are devoid of keratin and begin to accumulate more and more of this protein as they pass from one epidermal layer to another. This process is accelerated in the case of injuries, such as abrasions and burns [8].

Melanocytes are cells with long and thin processes, called dendrites, placed between the keratinocytes. They correspond to 8% of skin cells and release melanin pigment granules that are absorbed by the keratinocytes. Once in keratinocytes, melanin forms a barrier around the core on the side facing the skin surface. In this way, melanin protects cellular DNA against the deleterious effects of ultraviolet radiation [9].

The Langerhans cells migrate to the epidermis from the bone marrow. They represent a small percentage of the total epidermis cells and participate in the immune response.

Merkel cells are located deeper in the epidermis, where they come into contact with sensory neurons; together with them, they participate in the sense of touch [10].

The dermis is the layer that lies just below the epidermis and receives the increased blood supply to the skin. Most skin appendages are in the dermis: apocrine glands, eccrine glands, and hair follicles. The dermis is a connective tissue containing collagen and elastic

fibers. Fibroblasts, macrophages, and adipocytes constitute the cellular component from the dermis. It has two layers: superficial or papillary and deep dermis or reticulate [11].

The superficial layer corresponds to only one-fifth of the total dermis. It contains fine elastic fibers. Its total area is increased by the presence of dermal papillae, which are finger-like projections towards the epidermis. In some dermal papillae, corpuscles of Meissner (touch-sensitive nerve endings) and also free nerves (responsible for sensations of heat, cold, pain, tickling, and itching) are present [12].

In the deepest layer of the dermis, the reticular region, tissue is observed as dense, irregular connective tissue, with bundles of collagen fibers and thicker elastic fibers. Among the bundles of collagen fibers, follicles, hair, sweat, and sebaceous glands, nerves and fat cells can be observed. The combination of collagen fibers and elastic fibers gives the dermis the properties of elasticity, strength, and extensibility. When tissue damage reaches the reticular dermis, grafts are usually necessary [13].

The deepest layer of the skin is called the hypodermis or subcutaneous layer. It contains a large amount of adipose tissue, sensitive receptors pressure (Pacinian corpuscles), and large blood vessels that supply the dermis. Fibers that come from the dermis cross the hypodermis and attach to tissues and underlying organs [14].

The skin possesses an excellent regenerative capacity due to the presence of various mesenchymal stem cells (MSCs) located in its appendages (hair follicles, sebaceous glands, and sweat glands) as well as in the basal layer [15]. These cells exhibit a high degree of plasticity and are arranged in distinct compartments known as niches, where they interact with neighboring cells and a specific extracellular matrix to determine their functions [16–18]. In the skin, three different niches of MSC have been identified: (i) the basal layer of the epidermis, (ii) the hair follicle bulb (present in mice, but not in humans), and (iii) the base of the sebaceous gland duct, which suggests the existence of a niche also in the duct of the sweat glands [19–21].

A wound is defined as damage to or discontinuity of the structural anatomy of the skin and the consequent loss of its normal functions. It can be a simple interruption of the epithelial integrity or it can be deeper, extending to the subcutaneous tissue, with damage to various structures, such as tendons, muscles, vessels, nerves, organs' parenchyma, and bones [22].

Healing consists of the reestablishment of the continuity of the epidermis, so that the tissue that differentiates it acts as a physical, chemical, and bacterial barrier, which is one of the skin's vital functions [1]. The healing process requires an integrated expression of several chemokines, cytokines, growth factors, and cell types that are present in the wound from tissue injury to the final healing events. Throughout this process, their expression varies temporally and quantitatively. They are produced by cells present at the wound site and act in paracrine and autocrine signaling [23].

Wound healing can happen by regeneration or through the reparation process. When regeneration occurs, the tissue for reconstruction is the same as that of the healthy tissue. This can be observed in the superficial epidermis, in the mucous membranes, or in fetal skin. In tissue repair, the wound is filled with fibrotic tissue and presents with scars [11,24].

Tissues have different healing times. Wounds can be classified as acute or chronic according to the way they establish and evolve. Acute wounds heal within the period expected and in a way that is hassle-free. Chronic wounds are those that do not fulfill the progression of the normal healing stages, and the damage established is not repaired in the expected order and time. Many factors can contribute to the interruption and consequent damage of normal healing: infection, tissue hypoxia, necrosis, and exudates. Excessive amounts of inflammatory cytokines can prolong one or more phases of the healing time, leading to wound chronicity [23].

After the injury has occurred, to reestablish the anatomical condition and function (that is, healing), the following steps are necessary in the affected tissues: coagulation and hemostasis, the inflammatory phase, the proliferative phase, and the remodeling phase. These phases are sequential, overlapping, and interdependent such that in different areas

of the same wound, distinct phases of the healing process can be observed. Thus, deficiency in any of the healing stages determines the failure of the event [25–27] (Figure 2).

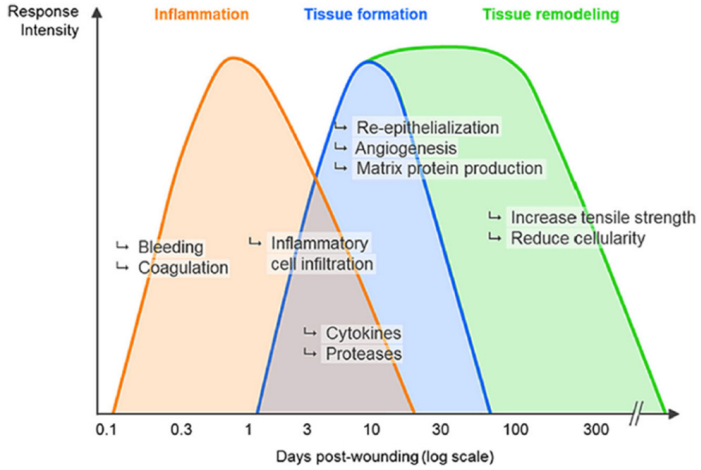


**Figure 2.** Temporal sequence illustrating the phases of epithelial healing. The diagram showcases the different phases that occur during the process of tissue regeneration and how they are interposed with one another.

Diabetes mellitus (DM) is an important global health problem caused by changes in nutritional habits, sedentary lifestyle, overweight, population growth and aging, increasing urbanization, and the greater survival of diabetic patients. It has a cost of billions of annual dollars that impacts the health systems of all countries, but it is more representative in underdeveloped countries. Type 1 diabetes is the carrier of exogenous insulin, while type 2 diabetes is more common and accounts for 85–90% of cases. Diabetes is characterized by disturbances in the secretion and action of insulin and can be managed with food control and physical exercise. Other less common types of diabetes have been reported, such as genetic defects of beta cells and of the insulin, degenerative diseases of the pancreas, diabetes related to other endocrinopathies, and drug diabetes. Complications include cardiovascular and cerebrovascular diseases, retinopathy, nephropathy, and ulcers and skin conditions [28]. Diabetic individuals have difficulty healing wounds in the extremities, especially in the feet. Diabetic foot (DF) wounds are caused by neuropathy and vascular insufficiency, with 20% having previous arterial occlusive disease, 50% having peripheral neuropathy, and 80% having both conditions. Any trauma leading to the formation of skin ulcers predisposes patients to complications [29,30]. Treatments for DF ulcers aim to increase vascularity and to break down physiological barriers that prevent healing, but the success of treatment depends on several factors. Chronic wounds of diabetic feet have their healing interrupted in the inflammatory phase due to deficiencies in cells involved in the process, as well as of chemokines, cytokines, and growth factors.

A possible countermeasure to treat chronic wounds in diabetic patients is the use of adult stem cells for tissue maintenance and repair [31]. Among them, mesenchymal stem cells (MSCs) are present throughout the organism and in the perivascular region of adult tissues. They are multipotent and capable of forming ectoderm, mesoderm, and endoderm cells [32], and they release exosomes to stimulate tissue regeneration and to regulate the immune system [33,34]. However, an important limitation of using MSCs lies in the necessity to cultivate cells, which involves enzymatic manipulation, leading additionally to an increase in the time to obtain them and the financial cost [35,36].

Rigenera® technology (Human Brain Wave, Turin, Italy) is now a currently available alternative technology for obtaining micrografts (namely progenitor cells (PCs) within their own extracellular matrix) involving disposable medical devices as mechanical disruptors of biological tissues [37–45]. It allows for obtaining micrografts in an autologous, homologous, and minimally invasive manner, and these can be used immediately without the need for

culture cells. Scientific studies have shown that the cellular population obtained after the mechanical disaggregation is positive for mesenchymal stem cells, with markers identifying those cells as PCs, and they have shown a viability ranging between 70 and 90%. AMTs have the ability to act both through cellular differentiation and in a paracrine manner through the release of secretomas containing various molecules that will act on neighboring cells; they have the potential to stimulate multiple events at once, allowing interdependent phases to be resolved endogenously [46].

In this study, diabetic foot wounds were used as an experimental model in order to verify the performance of AMTs in the evolution of the healing process in skin wounds. Fifty male Wistar rats were involved and divided into four groups: "control (C)"; "control treated with micrografts (CM)"; "diabetic (DB)"; and "diabetic treated with micrografts (DBM)".

## 2. Results

### *2.1. Histopathological Analysis*

Research findings on hematoxylin-eosin-stained slides revealed an extensive inflammatory infiltration among the granulation tissue seen in all groups at the start of healing (3 days). Nevertheless, the number of neutrophils in the CM group is substantially smaller (Figure 3). The images were acquired from samples collected 3 days after the creation of the artificial wound.

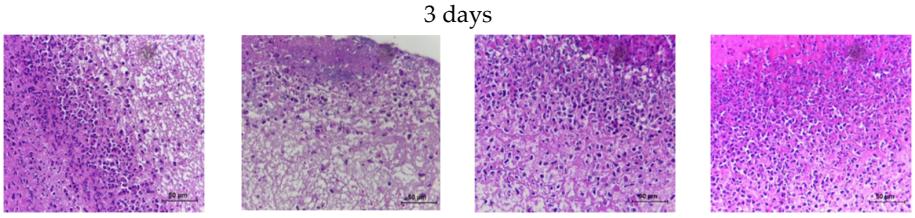


**Figure 3.** Photomicrograph showcasing the animals' skin on the third day of treatment. The image features the four different groups, namely (**a**) C "control", (**b**) CM "control treated with micrografts", (**c**) DB "diabetic", and (**d**) DBM "diabetic treated with micrografts". It is observed that all groups display an abundance of inflammatory cells, particularly degenerated neutrophils, within the granulation tissue. However, the CM group (**b**) exhibits a lower quantity of inflammatory cells compared to the C group. The staining utilized in the image is hematoxylin eosin (HE).

Despite the progression of the healing process, inflammatory cells remained in the diabetes groups (DB and DBM) longer than in the non-diabetic groups (C and CM) (Figure 4).

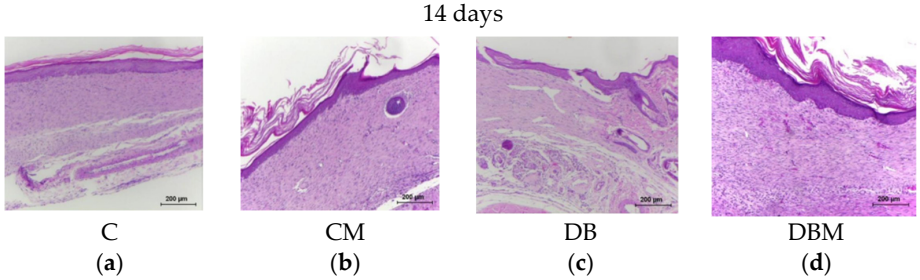


**Figure 4.** Photomicrograph displaying the animals' skin on the fourteenth day of treatment, featuring (**a**) C "control", (**b**) CM "control treated with micrografts", (**c**) DB "diabetic", and (**d**) DBM "diabetic treated with micrografts" groups. The image shows that the wound is completely re-epithelialized in all four groups. However, in the diabetic group (**c**), the lining epithelium is thinner and contains fewer layers in the stratum corneum. Additionally, collagen appears less organized in this group as compared to the others. Notably, the presence of persistent inflammatory cells is observed in the diabetic and diabetic groups treated with the micrograft.

According to histological studies, the CM group is in the healing phase after 3 days, which is equal to the C group after 7 days of recovery. At 7 days, the proliferation phase begins, leading to fibroblasts migration, angiogenesis, and the commencement of epithelialization (Figure 5).

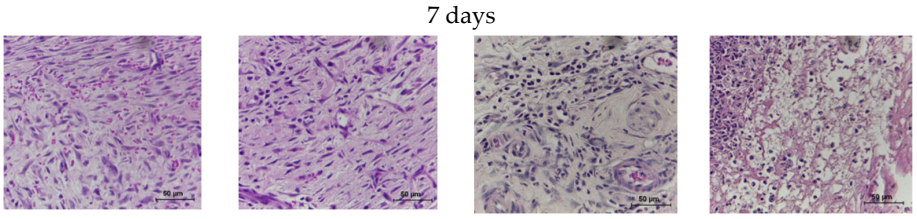


**Figure 5.** Photomicrograph displaying the animals' skin on the seventh day of treatment, featuring (**a**) C "control", (**b**) CM "control treated with micrografts", (**c**) DB "diabetic", and (**d**) DBM "diabetic treated with micrografts" groups. The image highlights the presence of hemorrhage and the formation of blood vessels in the C group. In the CM group, a greater quantity of fibroblasts and collagen fibers are observed in comparison to the C group. However, the presence of blood vessels and hemorrhage is lower in this group. In the DB group, an expressive presence of inflammatory cells is observed, which is also present in the DBM group. The staining utilized in the image is hematoxylin eosin (HE).

The epidermal tissue was detected at 3 days in the treatment groups (Figure 6), indicating a faster epithelialization in the micrograft groups.

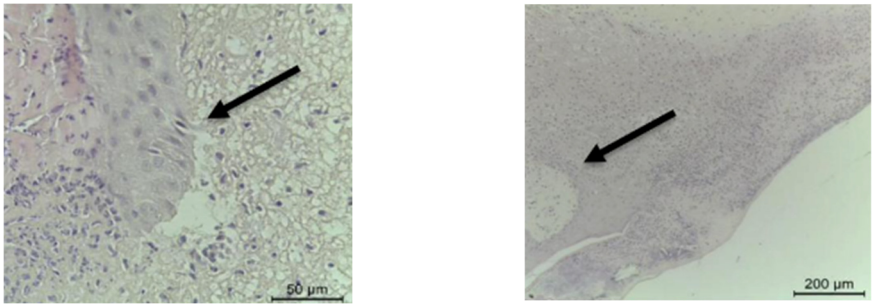


**Figure 6.** Photomicrograph showcasing the presence of lingual epithelial (indicated by an arrow) at three days in the CM "control treated with micrografts" group (**a**) and in the DBM "diabetic treated with micrografts" group (**b**). The staining technique employed in the image is hematoxylin eosin (HE).

Angiogenesis occurs in all groups; however, it takes longer to begin in the diabetic group, with detection occurring after just 7 days. Active fibroblasts were likewise discovered only after 7 days of recovery. The CM group has much more fibroblasts and collagen fiber production than the C group. Although there are still disordered regions, collagen is thicker than in the control group.

Granulation tissue with many newly formed capillaries and fibroblasts is present in the DBM group in the middle of the extracellular matrix formed by the newly formed fibrillar collagen synthetized. By 14 days (Figure 7), there was a full region of healing in all groups, with no discontinuity of the epidermis, and the healing was in the final phase of proliferation and the beginning of remodeling. Every layer of the epidermis is visible, from the stratum basale to the stratum cornea; however, the epidermis is thinner and has fewer keratin layers in the diabetic group. The formation of epidermal attachments has begun in the groups treated with the micrograft, but it is still lacking in the untreated groups. Granulation tissue has already been totally replaced by collagen, although collagen remains

fibrillar, with thin and disordered fibers, with an appearance of newly formed collagen in the diabetic group. The majority of fibroblasts have already been replaced by fibrocytes.

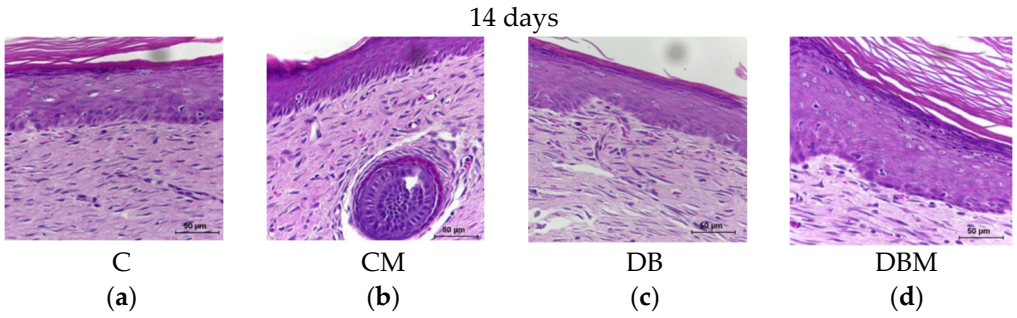


**Figure 7.** Photomicrograph displaying the animals' skin on the fourteenth day of treatment, featuring (**a**) C "control", (**b**) CM "control treated with micrografts", (**c**) DB "diabetic", and (**d**) DBM "diabetic treated with micrografts" groups. The image demonstrates complete epithelialization of the wound in all groups. In the CM group (**b**), the formation of an epidermal annex is observed. In the DB group (**c**), a reduction in the thickness of the epidermis and keratin layers is observed. Conversely, in the DBM group (**d**), the epidermis is fully re-epithelialized, with several layers of keratin and keratohyalin granules. The staining technique employed in the image is hematoxylin eosin (HE).

### *2.2. Collagen and Elastic Fibers Quantification*

The animals in the C group had less collagen at 7 and 14 days of evolution than the DBM group, which was still at 3 days of healing. As a result, the DBM group produced more collagen in a shorter healing time than the C groups with longer healing times (Figure 8).

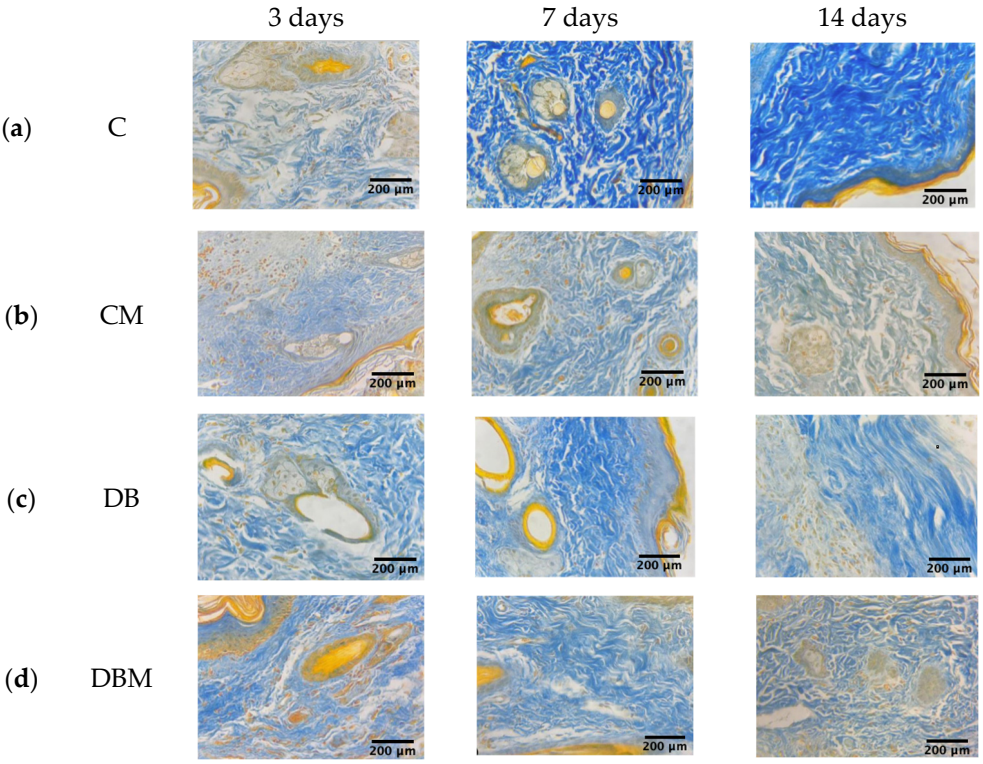


**Figure 8.** Photomicrograph displaying the rat skin with Mallory's trichrome for collagen quantification at 3, 7, and 14 days of healing evolution of (**a**) C "control", (**b**) CM "control treated with micrografts", (**c**) DB "diabetic", and (**d**) DBM "diabetic treated with micrografts" groups. The blue color represents collagen.

The morphometric analysis for elastic fibers quantification revealed no statistically significant differences between the groups (Figures 9 and 10).

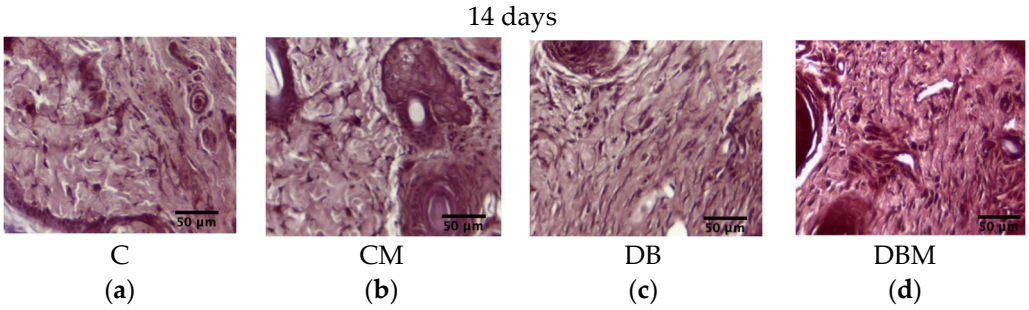


**Figure 9.** Microscopic images of nitric-orcein-stained mouse skin depicting elastic fiber quantification during the 14-day healing progression. (**a**) C "control", (**b**) CM "control treated with micrografts", (**c**) DB "diabetic", and (**d**) DBM "diabetic treated with micrografts".

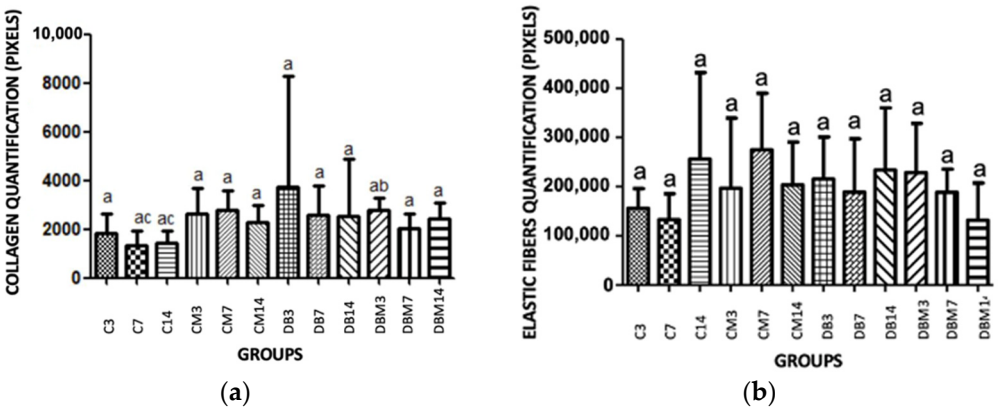


**Figure 10.** Statistical analysis of collagen production (**a**) and quantification of elastic fibers (**b**), measured using the Gimp 2.0 software. Statistical analyses were performed using the Kruskal–Wallis test with post hoc Dunn. Means denoted by the same letter do not exhibit significant differences ($p < 0.05$). The different groups analyzed include the C group (control), CM group (control treated with micrografts), DB group (diabetic), and DBM group (diabetic treated with micrografts).

From the statistical analysis conducted to quantify collagen production and elastic fibers, it was found that there is a statistical difference between C (7 days) and C (14 days) compared to DBM (3 days) for collagen (Figure 10a). However, no statistically significant differences were observed among the groups for elastic fibers (Figure 10b).

### *2.3. Immunohistochemical Analysis for COL1, COL3, VEGF-A, IL4, and IL10*

Throughout the 3-day assessment, there were no significant changes in collagen I labeling. At 7 days, the CM group had more COL1 marking than the C group. The animals in the DB and DBM groups had the lowest marking and did not distinguish from one another. At 14 days, the same behavior was seen (Figure 11a).

At the 3-day assessment, there were no significant changes in collagen III labeling. At 7 days, tissues in the C and CM groups had more marking in their fragments, followed by the animals in the DBM group. The animals in the DB group had the least amount of staining. The animals in the CM and DBM groups had more marking at 14 days than the C and DB groups, with the latter having the lowest average (Figure 11b).

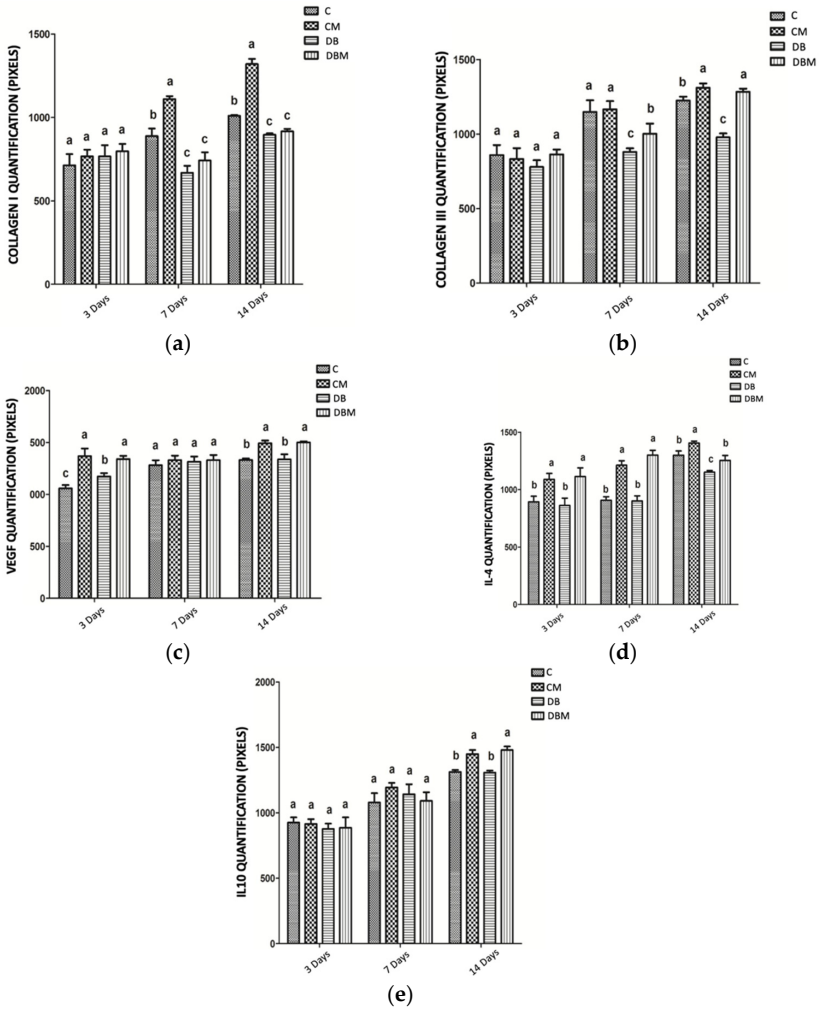


**Figure 11.** The different groups statistically analyzed include C "control", CM "control treated with micrografts", DB "diabetic", and DBM "diabetic treated with micrografts". (**a**) Pixel-based quantification of collagen I in skin tissue samples obtained from experimental animal groups. Tukey and Kramer Multiple Comparisons tests revealed no significant differences ($p > 0.05$) among means marked with the same letter. (**b**) Pixel-based quantification of collagen III in skin tissue samples obtained from experimental animal groups. Tukey and Kramer Multiple Comparisons tests revealed no significant differences ($p > 0.05$) among means marked with the same letter. (**c**) Pixel-based quantification of VEGF in skin tissue samples obtained from experimental animal groups. Tukey and Kramer Multiple Comparisons tests revealed no significant differences ($p > 0.05$) among means marked with the same letter. (**d**) Pixel-based quantification of IL4 in skin tissue samples obtained from experimental animal groups. Tukey and Kramer Multiple Comparisons tests revealed no significant differences ($p > 0.05$) among means marked with the same letter. (**e**) Pixel-based quantification of IL10 in skin tissue samples obtained from experimental animal groups. Tukey and Kramer Multiple Comparisons tests revealed no significant differences ($p > 0.05$) among means marked with the same letter.

At 3 days, there were significant variations in the evaluation of VEGF, with skin samples from the CM and DBM groups demonstrating higher marking than the DB and C groups, with the latter showing the lowest markup. There were no variations in marking between the experimental groups after 7 days. By 14 days, however, the animals in the CM and DBM groups had more markings than the C and DB groups, which did not differ from each other (Figure 11c).

We observed the same trend at the 3- and 7-day evaluations, characterized by increased marking in the skin pieces of the CM and DBM animals, whereas the C and DB groups

showed less staining without significant differences. The animals in the CM group, on the other hand, had more marking at 14 days. The animals in the C and DBM groups did not vary from one another, but the DB had less marking (Figure 11d).

During 3 and 7 days, there was no significant change in the labeling of this cytokine. By 14 days, however, the animals in the CM and DBM groups had more marking. The animals in the C and DB groups had less marking but did not vary from one another (Figure 11e).

### *2.4. Evaluation of the Oxidative Stress—Measurement of Gluthatione (GSH)*

Tissue assessment of GSH levels at three points in the groups' studies revealed that the groups treated with the micrograft had greater levels than the diabetic group (Figure 12a). In terms of tissue concentrations of skin lipid peroxidation (TBARS) levels, the DB group showed a substantial rise, but the DBST group showed a decrease when compared to the diabetic and control groups (Figure 12b).

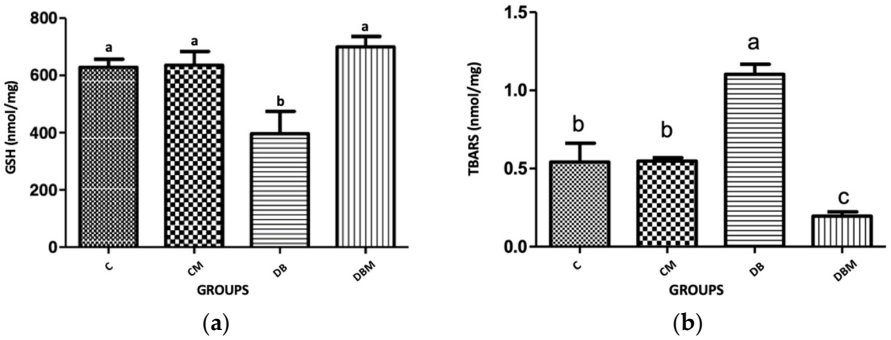


**Figure 12.** Graphs showing GSH and TBARS values in the skin of animals belonging to different experimental groups (nmol/mg of protein) on the 14th day of treatment. The experimental groups include the C (control group), the CM (control group treated with AMGs), the DB (diabetic group), and the DBM (diabetic group treated with AMTs). Statistical significance was determined by the Kruskal–Wallis test with Dunn's post hoc analysis. Means sharing the same letter are not significantly different from each other. (**a**) GSH; (**b**) TBARS.

### *2.5. Evaluation of Tumor Necrosis Factor-α (TNF-α)*

In terms of TNF-α dose, the control group (C) had a greater concentration than the other experimental groups on the third day. However, on the seventh and fourteenth days, the diabetic (DB) group had a greater concentration, contrasting with the other groups' findings (Figure 13).

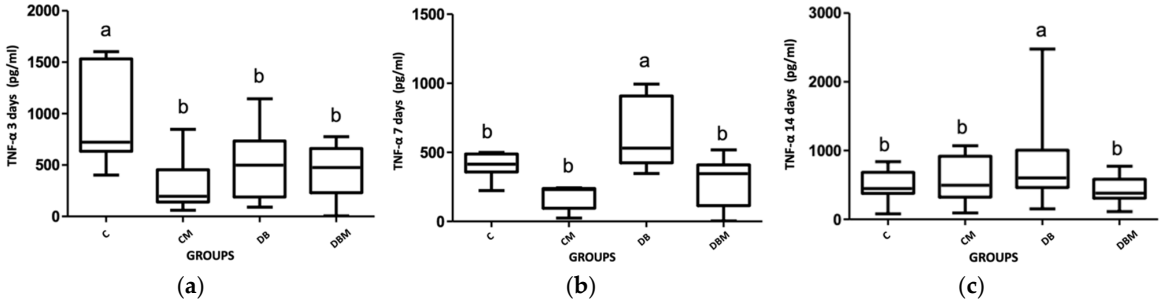


**Figure 13.** The graphs display the TNF-α values in the skin of animals belonging to different experimental groups (pg/mL), including the C (control group), the CM (control group treated with AMGs), the DB (diabetic group), and the DBM (diabetic group treated with AMTs). The y axis shows the different treatment times, which are labeled as the 3rd treatment time, 7th treatment time, and 14th treatment time. The statistical analysis was performed using the Kruskal–Wallis test with Dunn's post hoc test. Means with the same letter are not significantly different from each other. (**a**) TNF-α 3 days; (**b**) TNF-α 7 days; (**c**) TNF-α 14 days.

## 3. Discussion

The process of tissue healing involves a series of events that are interdependent and involve various chemokines, cytokines, and growth factors produced by cells that participate in tissue repair [11,23–25]. This process goes through phases of coagulation and hemostasis, inflammation, proliferation, and tissue remodeling [24]. In extremity wounds of diabetic individuals, the healing process is interrupted in the inflammatory phase due to a large amount of cytokines, chemokines, and pro-inflammatory factors that prevent progression to the proliferation phase and result in chronic wounds [47].

Stem cells are seen as a possible solution to this problem as they can release exosomes containing factors that positively interfere in healing and also differentiate into other cell types, which can act on stagnant healing and act on several factors simultaneously [48].

Micrografts containing progenitor cells have been shown to induce a faster evolution of the wound healing process [49]. Animals treated with micrografts present at 3 days a histological appearance similar to those at 7 days that did not receive the micrograft.

The presence of neutrophils in the proliferation and remodeling phases has been shown to be a characteristic of diabetic animals, which was different from the control group. This finding may be due to the greater number of inflammatory cytokines in diabetics, which attract a greater number of neutrophils to the lesion.

The skin wound samples for histopathological analysis were collected three, seven, and fourteen days after creating the artificial wounds for several reasons, which can be justified based on the wound healing process and recent scientific studies. Firstly, this multi-time-point approach allows for a more comprehensive assessment of the dynamic changes that occur during different phases of wound healing. The three-day time stop captures the early inflammatory phase, characterized by acute inflammation, immune cell infiltration, and the initiation of tissue repair processes. By collecting samples at this time point, the initial response to the wound and the early cellular and molecular events can be monitored. The seven-day time stop represents the proliferative phase, during which granulation tissue formation, angiogenesis, and collagen synthesis occur. It is a crucial period for cell proliferation, migration, and extracellular matrix deposition. Collecting samples at this time point enables the evaluation of tissue regeneration and the progression of healing. The fourteen-day mark corresponds to the remodeling phase, characterized by collagen remodeling, wound contraction, and the maturation of the newly formed tissue. By collecting samples at this time point, the structural and functional changes that occur during this critical phase of wound healing can be assessed [25,50,51].

The quantification of collagen production through staining showed that collagen production was more effective in animals treated with micrografts at 3 days of healing compared to those at 7 and 14 days of evolution of control animals. The elastic fibers present in the skin showed no significant difference among the groups studied with regard to fiber production elasticity.

Angiogenesis is the process by which new blood vessels are formed from preexisting vessels in the tissue. VEGF is a potent stimulator of this process, and increased expression of VEGF indicates that blood vessel formation is active, which is important for cell growth and proliferation as well as the formation of granulation tissue. In this study, it was found that at 3 days of healing, VEGF was increased in the groups treated with micrografts compared to the untreated groups, indicating an earlier recovery of vascularization in the CM and DBM groups and favoring faster healing.

Overall, micrografts containing progenitor cells have been shown to accelerate and produce collagen in greater quantities than the control group with longer healing time, resulting in scar tissue with better collagen organization.

Cytokines are proteins that bind to cell membrane receptors and induce their biological effects. The action of cytokines can be autocrine, paracrine, or endocrine. TNF-$\alpha$ is a cytokine produced by macrophages, lymphocytes, and monocytes. Its main physiological effect is to promote immune and inflammatory responses through the recruitment of neutrophils and monocytes to the site of infection and the activation of these cells [52].

TNF-α is present in chronic wounds, such as those present in diabetic feet. In wounds that heal under normal conditions, TNF-α decreases as the cells that produce it are eliminated from the inflammatory process. However, in the wounds of diabetic feet, TNF-α tends to remain at high levels. The treatment with micrografts showed a reduction in TNF-α in diabetic animals compared to those who were also diabetic but did not receive treatment. Thus, the applied micrograft helped to reduce this cytokine, and, consequently, its inflammatory effects.

In addition to pro-inflammatory cytokines, anti-inflammatory cytokines are also important regulators of healing. IL-4 is a cytokine with anti-inflammatory characteristics that is produced mainly by mast cells, eosinophils, Th2 cells, and basophils. IL-4 works in tissue homeostasis by changing macrophages from the M1 profile (pro-inflammatory) to the M2 profile (anti-inflammatory) [53]. Up to 7 days of healing, IL-4 maintained its highest levels in the groups treated with the micrograft. In this phase, inflammatory cells were present from the wound, including macrophages. Therefore, IL-4 may have activated the macrophage alternative pathway for the M2 profile, contributing to the reduction of inflammation. IL-4 is also able to promote the repair of epithelial wounds in vitro by reducing the cytokine-induced epithelial barrier defects.

The importance of IL-10 in wound healing lies in its limitation and termination of inflammatory responses. IL-10 inhibits the infiltration of neutrophils and macrophages into the lesion, as well as the expression of various pro-inflammatory chemokines and cytokines [54]. In this study, at 3 and 7 days after injury, there was no significant difference in IL-10 production among the groups studied. Only at 14 days of healing was IL-10 increased in the groups treated with micrografts compared to the untreated groups. The two together, IL-4 and IL-10, being anti-inflammatory in nature, maintain a favorable environment for healing throughout the healing process. IL-10 is also capable of inhibiting TNF-α. In fact, IL-10 was higher at 14 days in the micrograft-treated groups at the same time that TNF-α was lower in these same groups.

Oxidative stress is the result of an increase in reactive oxygen species (ROS) and/or reactive nitrogen species (RNS) as a result of a constant imbalance between the production of reactive molecules (mainly ROS and RNS) and antioxidant agents [55]. The level of TBARS is pointed out as an effective method to identify these radicals, and high levels of TBARS are present in patients with complications of diabetes mellitus. The level of TBARS was shown to be significantly increased in the DB group compared to the DBM and CM groups.

## 4. Materials and Methods

### *4.1. Animal Model*

Fifty male Wistar rats (90 days old, weighing around 300 ± 30 g) from the Department of Animal Morphology and Physiology, Rural Federal University of Pernambuco, were involved in this study. The project was submitted to the institutional ethics committee and approved under protocol number 23082.014335/2018–85 and license No. 89/2018.

These animals were kept in cages, with food and water ad libitum, at a temperature of 22 ± 1 °C and with artificial lighting that established a photoperiod of 12 h of light and 12 of dark hours, considering the light period from 06:00 to 18:00 h. The animals were randomly divided into 4 groups, namely: control (C) ($n$ = 10); control treated with micrografts (CM) ($n$ = 10); diabetic (DB) ($n$ = 15); and diabetic treated with micrografts (DBM) ($n$ = 15).

### *4.2. Diabetes Induction*

Diabetes was induced in the animals of the DB and DBM groups by intraperitoneal administration of Streptozotocin solution (Sigma Chemical Co., St. Louis, MO, USA) after a 14 h fasting period. Diabetes was confirmed on the seventh day after the application. Streptozotocin was diluted in 10 mM sodium citrate buffer (pH 4.5) and administered in a single dose of 60 mg/kg of animal weight. The C and CM groups received, in the same

way, equivalent doses of saline solution. After 30 min from administration, all animals were fed normally [56].

Only animals with blood glucose above 200 mg/dL (Accu-Chek Activ Kit Glucometer, Roche Diabates Care, Indianapolis, IN, USA) were included in this study, except for the control groups.

### *4.3. Wound Preparation*

The lesions were performed on the backs of the left hind legs of the rats, with a sterile scalpel, in order to remove the skin and subcutaneous tissue until exposure of the muscle tendons (Figure 14).

**Figure 14.** A lesion was performed on the left hind legs of the animals, which involved the removal of the overlying skin and subcutaneous tissue to expose the underlying muscle tendons. The resulting lesion area measured approximately 1 $cm^2$.

### *4.4. Autologous Micrografts Rigenera® Technology*

AMGs were obtained utilizing a Class II medical device, called Rigeneracons, that consists of a grid with six micro-blades encircling hundreds of holes that are 80 µm in diameter, allowing the selection of AMGs with exact sizes using a dimensional exclusion method. An electrical motor, known as Sicurdrill, drives the mechanical fragmentation (Figure 15). Many soft and hard tissues, including the dermis, cartilage, bone, fat, and heart tissues, may be swiftly and effectively broken down using the technology. The AMG solution can be injected around the margins and the bed of a wound or used to imbibe a dermal substitute. Because the AMG technology does not require the use of enzymes or other chemicals, the operation takes only 30 min to complete.

(**a**) (**b**)

**Figure 15.** After shaving, a skin incision was made on the animal's back (**a**). The skin fragment was subsequently cut into smaller pieces, as shown in image (**b**), before being placed into the Rigeneracons device for processing.

### *4.5. Histopathological Analysis*

The animals in both the experimental and control groups were sedated with ketamine hydrochloride (80 mg/kg) and xylazine (6.0 mg/kg) intramuscularly three, seven, and fourteen days after the artificial wounds creation. The wound skin was collected by a rectangular incision around the lesion (Figure 16). The rats were then euthanized with 100 mg/kg sodium thiopental.

**Figure 16.** A skin fragment was collected for analysis, ensuring a sufficient safety margin around the wound. Half of the fragment was fixed in buffered formalin, while the other half was frozen at −20 °C for subsequent analysis.

Half of the material was fixed in buffered formalin for 48 h before being paraffin embedded. The sections were stained with hematoxylin and eosin, Mallory's trichrome, and nitric orcein for histological investigation using a light microscope (OLYMPUS BX-50, Tokyo, Japan). The other half was frozen at −20 °C in a freezer.

Samples for histological analysis were collected at three, seven, and fourteen days following the injury.

### *4.6. Collagen and Elastic Fibers Quantification*

Histological slices were stained with Mallory's trichrome and nitric orcein, respectively, to quantify the collagen and elastic fibers. For this purpose, three slides were utilized for each group, with five fields captured on each slide. The images were captured with a Sony® (Tokyo, Japan) video camera attached to an Olympus® (Tokyo, Japan) Bx50 microscope and submitted to the Gimp 2.0 application for quantification using the RGB Histogram (Red-Green-Blue), which is based on luminescence intensity and where the tones of the image pixels vary from 0 to 255, with tone 0 representing absolute darkness (lowest luminescence) and tone 255 representing absolute white (higher luminescence) [57].

### *4.7. Immunohistochemical Analysis for COL1, COL3, VEGF-A, IL4, and IL10*

COL1A1 (sc-293182, Santa Cruz Biotechnology, Santa Cruz, CA, USA), COL3A1 (sc-271249, Santa Cruz Biotechnology, Santa Cruz, CA, USA), VEGF-A (MBS2540134, MyBioSource, San Diego, CA, USA), IL-4 (sc-53084, Santa Cruz Biotechnology, Santa Cruz, CA, USA), and IL-10 (sc-365858, Santa Cruz Biotechnology, Santa Cruz, CA, USA) antibodies in a 1:100 dilution ratio were used.

The slides were deparaffinized and rehydrated in xylene and alcohols, respectively. The antigen recovery was carried out in the microwave for 5 min at high temperature with a citrate buffer solution (pH 8.0). Endogenous peroxidase was inhibited by a 3% hydrogen peroxide in methanol solution [58]. The nonspecific antigen–antibody interaction was inhibited by incubating the slides in PBS and 5% bovine serum albumin (BSA) for 1 h. All antibodies were diluted in PBS/BSA 1% overnight. The parts were then treated with Histofine® (Cod. 414191F—Nichirei Biosciences, Tokyo, Japan) for 30 min. The antigen–antibody reaction was detected as a brown precipitate after four minutes of treatment with 3,3 diaminobenzidine and counterstained with hematoxylin. A video camera (Sony) coupled with the Olympus BX-50 microscope was used to collect the images.

### *4.8. Evaluation of the Oxidative Stress—Measurement of Gluthatione (GSH)*

The skin's oxidative stress was assessed by measuring lipid peroxidation and GSH levels. The quantities of acid reactive chemicals thiobarbiturate (TBARS) were used to estimate lipid peroxidation (Figure 17), whereas non-protein sulfhydryl groups were used to estimate reduced GSH (Figure 18) [59,60]. Skin pieces were macerated in 1.15% KCl in a proportion of 10 mL/1 g until completely homogenized. The homogenate was transferred to a test tube, and 2 mL of the reagent (0.375% thiobarbituric acid and 75% acid trichloroacetic acid) was added for every mL of the mixture. Duplicate tubes were sealed and heated in a

water bath (100 °C) for 15 min. The supernatant was separated, and the absorbance was measured at 535 nm [61].

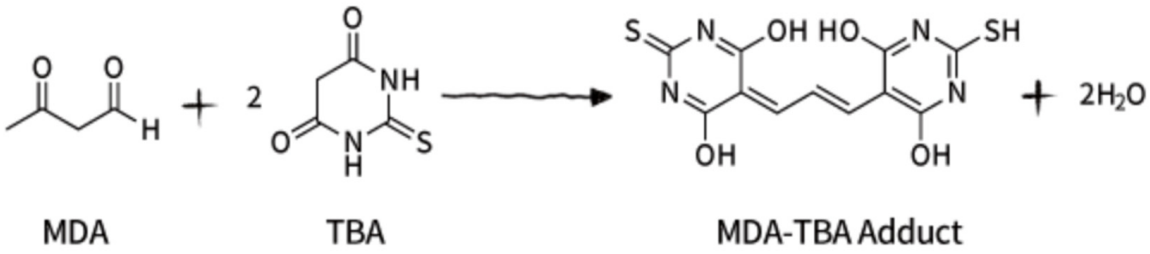


**Figure 17.** Lipid peroxidation is a widely recognized cellular injury mechanism in both plants and animals, often used as an indicator of oxidative stress in cells and tissues. Polyunsaturated fatty acids give rise to unstable lipid peroxides, which subsequently decompose to form a range of complex compounds, including reactive carbonyl compounds like malondialdehyde (MDA). Thiobarbituric acid reactive substances (TBARS) measurement is a well-established screening and monitoring method for lipid peroxidation. In this method, MDA in the sample reacts with thiobarbituric acid (TBA) to form the MDA–TBA adduct, which can be quantified colorimetrically at 532 nm. This analytical approach relies on the reaction of MDA with TBA, a chromogenic reagent, at a constant temperature of 25 °C.

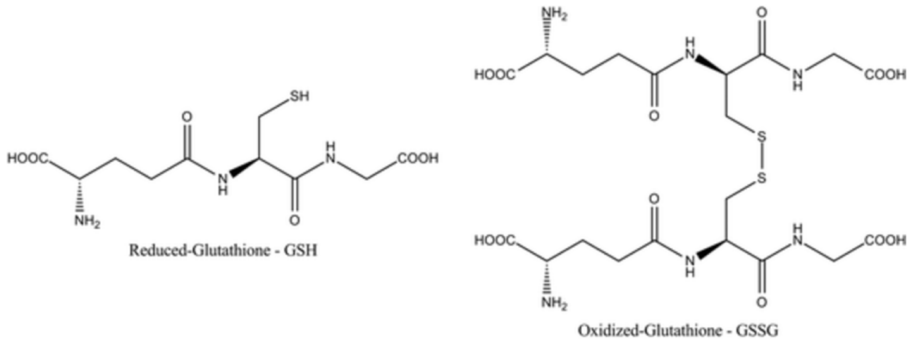


**Figure 18.** Glutathione is a tripeptide that exists in two forms: reduced (GSH) and oxidized (GSSG). The ratio of GSH to GSSG within cells is a widely used marker of cellular oxidative stress, as an increased GSSG-to-GSH ratio indicates greater oxidative stress. GSH acts as an important antioxidant by neutralizing (reducing) reactive oxygen species, protecting cells from oxidative damage.

### *4.9. Evaluation of Tumor Necrosis Factor-α (TNF-α)*

TNF-α dose was determined using the ELISA method, according to the manufacturer's instructions (RAB0479-1KT—Sigma-Aldrich (St. Louis, MO, USA)) [62].

### *4.10. Statistical Analysis*

Statistical analysis was conducted using the Kruskal–Wallis test with post hoc Dunn analysis to assess collagen production and quantification of elastic fibers utilizing Gimp 2.0 software. The significance level was set at $p < 0.05$.

Regarding collagen I quantification, pixel-based analysis was performed on skin tissue samples from the animal groups. Tukey and Kramer Multiple Comparisons tests showed no significant differences ($p > 0.05$) among means labeled with the same letter.

Similarly, pixel-based quantification of collagen III, VEGF, IL4, and IL10 in skin tissue samples showed no significant differences ($p > 0.05$) among means marked with the same letter.

For GSH and TBARS values, statistical significance was determined using the Kruskal–Wallis test with Dunn's post hoc analysis ($p < 0.05$). Means sharing the same letter were not significantly different from each other.

The analysis of TNF-α values in the skin of animals across different experimental groups and treatment times was performed using the Kruskal–Wallis test with Dunn's post hoc test ($p < 0.05$). Means with the same letter were not significantly different from each other.

The software used for statistical analysis was GraphPad Prism 9.0.0.

## 5. Conclusions

Autologous micrografts have demonstrated effectiveness in promoting healing of difficult-to-heal wounds by influencing epithelialization, angiogenesis, and collagen production. Treatment with AMG has been observed to reduce tissue inflammation, resulting in improved healing in animals with and without diabetes.

**Author Contributions:** Conceptualization, M.B.P., F.N., A.G. and A.F.S.; methodology, M.B.P. and I.M.F.d.M.; validation, M.B.P. and A.F.S.; formal analysis, M.B.P. and I.M.F.d.M.; investigation, M.B.P.; resources, F.D.A.L.S., Á.A.C.T. and L.D.V.; data curation, M.B.P. and I.M.F.d.M.; writing—original draft preparation, M.B.P. and E.P.; writing—review and editing, M.B.P., E.P. and A.F.S.; visualization, M.B.P. and E.P.; supervision, F.N. and A.F.S.; project administration, A.F.S.; funding acquisition, A.F.S. All authors have read and agreed to the published version of the manuscript.

**Funding:** This research was funded by CAPES (Coordenação de Aperfeiçoamento de Pessoal de Nível Superior), Brazil and Human Brain Wave, Italy.

**Institutional Review Board Statement:** The animal study protocol was approved by the Ethics Committee of the Rural Federal University of Pernambuco, protocol code 89/2018, process 23082.014335/2018-85, approval in 22 August 2018.

**Informed Consent Statement:** Not applicable.

**Data Availability Statement:** Not applicable.

**Conflicts of Interest:** E.P. belongs to the R&D department of HBW srl, the company owner of the Rigenera Micrografting Technology. A.G. holds the position of Chief Executive Officer at HBW srl. The remaining authors declare that the research was conducted in the absence of any commercial or financial relationships that could be construed as a potential conflict of interest.

## References

1. Rittié, L. Cellular mechanisms of skin repair in humans and other mammals. *J. Cell Commun. Signal.* **2016**, *10*, 103–120. [CrossRef]
2. Blair, M.J.; Jones, J.D.; Woessner, A.E.; Quinn, K.P. Skin Structure–Function Relationships and the Wound Healing Response to Intrinsic Aging. *Adv. Wound Care* **2020**, *9*, 127–143. [CrossRef] [PubMed]
3. Shen, Z.; Sun, L.; Liu, Z.; Li, M.; Cao, Y.; Han, L.; Wang, J.; Wu, X.; Sang, S. Rete ridges: Morphogenesis, function, regulation, and reconstruction. *Acta Biomater.* **2023**, *155*, 19–34. [CrossRef] [PubMed]
4. Goleva, E.; Berdyshev, E.; Leung, D.Y.M. Epithelial barrier repair and prevention of allergy. *J. Clin. Investig.* **2019**, *129*, 1463–1474. [CrossRef] [PubMed]
5. Pontiggia, L.; Ahuja, A.K.; Yosef, H.K.; Rütsche, D.; Reichmann, E.; Moehrlen, U.; Biedermann, T. Human Basal and Suprabasal Keratinocytes Are Both Able to Generate and Maintain Dermo–Epidermal Skin Substitutes in Long-Term In Vivo Experiments. *Cells* **2022**, *11*, 2156. [CrossRef]
6. Nguyen, A.V.; Soulika, A.M. The Dynamics of the Skin's Immune System. *Int. J. Mol. Sci.* **2019**, *20*, 1811. [CrossRef]
7. Gantwerker, E.A.; Hom, D.B. Skin: Histology and Physiology of Wound Healing. *Clin. Plast. Surg.* **2012**, *39*, 85–97. [CrossRef] [PubMed]
8. Piipponen, M.; Li, D.; Landén, N.X. The Immune Functions of Keratinocytes in Skin Wound Healing. *Int. J. Mol. Sci.* **2021**, *21*, 8790. [CrossRef] [PubMed]
9. Yardman-Frank, J.M.; Fisher, D.E. Skin pigmentation and its control: From ultraviolet radiation to stem cells. *Exp. Dermatol.* **2020**, *30*, 560–571. [CrossRef]
10. Rippa, A.L.; Kalabusheva, E.P.; Vorotelyak, E.A. Regeneration of Dermis: Scarring and Cells Involved. *Cells* **2019**, *8*, 607. [CrossRef]
11. Woodley, D.T. Distinct Fibroblasts in the Papillary and Reticular Dermis. *Dermatol. Clin.* **2017**, *35*, 95–100. [CrossRef] [PubMed]
12. Piccinin, M.A.; Miao, J.H.; Schwartz, J. *Histology, Meissner Corpuscle*; StatPearls Publishing: Treasure Island, FL, USA, 2023.
13. Losquadro, W.D. Anatomy of the Skin and the Pathogenesis of Nonmelanoma Skin Cancer. *Facial Plast. Surg. Clin. N. Am.* **2017**, *25*, 283–289. [CrossRef] [PubMed]
14. Takeo, M.; Lee, W.; Ito, M. Wound Healing and Skin Regeneration. *Cold Spring Harb. Perspect. Med.* **2015**, *5*, a023267. [CrossRef] [PubMed]

15. Yuan, T.; Yang, T.; Chen, H.; Fu, D.; Hu, Y.; Wang, J.; Yuan, Q.; Yu, H.; Xu, W.; Xie, X. New insights into oxidative stress and inflammation during diabetes mellitus-accelerated atherosclerosis. *Redox Biol.* **2019**, *20*, 247–260. [CrossRef]
16. Wong, T.C.; Piehler, K.; Meier, C.G.; Testa, S.M.; Klock, A.M.; Aneizi, A.A.; Shakesprere, J.; Kellman, P.; Shroff, S.G.; Schwartzman, D.S.; et al. Association Between Extracellular Matrix Expansion Quantified by Cardiovascular Magnetic Resonance and Short-Term Mortality. *Circulation* **2012**, *126*, 1206–1216. [CrossRef]
17. Gattazzo, F.; Urciuolo, A.; Bonaldo, P. Extracellular matrix: A dynamic microenvironment for stem cell niche. *Biochim. Biophys. Acta* **2014**, *1840*, 2506–2519. [CrossRef]
18. Assis-Ribas, T.; Forni, M.F.; Winnischofer, S.M.B.; Sogayar, M.; Trombetta-Lima, M. Extracellular matrix dynamics during mesenchymal stem cells differentiation. *Dev. Biol.* **2018**, *437*, 63–74. [CrossRef] [PubMed]
19. Hsu, Y.-C.; Fuchs, E. A family business: Stem cell progeny join the niche to regulate homeostasis. *Nat. Rev. Mol. Cell Biol.* **2012**, *13*, 103–114. [CrossRef]
20. Hsu, Y.-C.; Li, L.; Fuchs, E. Emerging interactions between skin stem cells and their niches. *Nat. Med.* **2014**, *20*, 847–856. [CrossRef] [PubMed]
21. Fuchs, E.; Blau, H.M. Tissue Stem Cells: Architects of Their Niches. *Cell Stem Cell* **2020**, *27*, 532–556. [CrossRef]
22. Atiyeh, B.S.; Abbas, J.; Costagliola, M. Barreira cutânea para reconstrução mamária com prótese. *Rev. Bras. Cir. Plástica* **2012**, *27*, 630–635. [CrossRef]
23. Velnar, T.; Bailey, T.; Smrkolj, V. The Wound Healing Process: An Overview of the Cellular and Molecular Mechanisms. *J. Int. Med. Res.* **2009**, *37*, 1528–1542. [CrossRef]
24. Reinke, J.; Sorg, H. Wound Repair and Regeneration. *Eur. Surg. Res.* **2012**, *49*, 35–43. [CrossRef]
25. Eming, S.A.; Martin, P.; Tomic-Canic, M. Wound repair and regeneration: Mechanisms, signaling, and translation. *Sci. Transl. Med.* **2014**, *6*, 265–266. [CrossRef] [PubMed]
26. Forbes, J.M.; Cooper, M.E. Mechanisms of Diabetic Complications. *Physiol. Rev.* **2013**, *93*, 137–188. [CrossRef]
27. Boniakowski, A.E.; Kimball, A.S.; Jacobs, B.N.; Kunkel, S.L.; Gallagher, K.A. Macrophage-Mediated Inflammation in Normal and Diabetic Wound Healing. *J. Immunol.* **2017**, *199*, 17–24. [CrossRef]
28. GBD 2016 Disease and Injury Incidence and Prevalence Collaborators. Global, regional, and national incidence, prevalence, and years lived with disability for 328 diseases and injuries for 195 countries, 1990–2016: A systematic analysis for the Global Burden of Disease Study 2016. *Lancet* **2017**, *390*, 1211–1259. [CrossRef] [PubMed]
29. Bandyk, D.F. The diabetic foot: Pathophysiology, evaluation, and treatment. *Semin. Vasc. Surg.* **2018**, *31*, 43–48. [CrossRef]
30. Patel, S.; Srivastava, S.; Singh, M.R.; Singh, D. Mechanistic insight into diabetic wounds: Pathogenesis, molecular targets and treatment strategies to pace wound healing. *Biomed. Pharmacother.* **2019**, *112*, 108615. [CrossRef]
31. Wan, C.-D.; Cheng, R.; Wang, H.-B.; Liu, T. Immunomodulatory effects of mesenchymal stem cells derived from adipose tissues in a rat orthotopic liver transplantation model. *Hepatobiliary Pancreat. Dis. Int.* **2008**, *7*, 29–33.
32. Mafi, P. Adult Mesenchymal Stem Cells and Cell Surface Characterization—A Systematic Review of the Literature. *Open Orthop. J.* **2011**, *5*, 253–260. [CrossRef] [PubMed]
33. Waszak, P.; Alphonse, R.S.; Vadivel, A.; Ionescu, L.; Eaton, F.; Thébaud, B.; Abreu, S.C.; Weiss, D.J.; Rocco, P.R.M.; Rüdiger, M.; et al. Preconditioning Enhances the Paracrine Effect of Mesenchymal Stem Cells in Preventing Oxygen-Induced Neonatal Lung Injury in Rats. *Stem Cells Dev.* **2012**, *21*, 2789–2797. [CrossRef]
34. Phinney, D.G.; Pittenger, M.F. Concise Review: MSC-Derived Exosomes for Cell-Free Therapy. *Stem Cells* **2017**, *35*, 851–858. [CrossRef] [PubMed]
35. Ferrin, I.; Beloqui, I.; Zabaleta, L.; Salcedo, J.M.; Trigueros, C.; Martin, A.G. Isolation, Culture, and Expansion of Mesenchymal Stem Cells. In *Stem Cell Banking*; Humana Press: New York, NY, USA, 2017; pp. 177–190. [CrossRef]
36. Wang, C.; Börger, V.; Sardari, M.; Murke, F.; Skuljec, J.; Pul, R.; Hagemann, N.; Dzyubenko, E.; Dittrich, R.; Gregorius, J.; et al. Mesenchymal Stromal Cell–Derived Small Extracellular Vesicles Induce Ischemic Neuroprotection by Modulating Leukocytes and Specifically Neutrophils. *Stroke* **2020**, *51*, 1825–1834. [CrossRef]
37. Baena, R.R.Y.; D'Aquino, R.; Graziano, A.; Trovato, L.; Aloise, A.C.; Ceccarelli, G.; Cusella, G.; Pelegrine, A.A.; Lupi, S.M. Autologous Periosteum-Derived Micrografts and PLGA/HA Enhance the Bone Formation in Sinus Lift Augmentation. *Front. Cell Dev. Biol.* **2017**, *5*, 87. [CrossRef] [PubMed]
38. Ceccarelli, G.; Presta, R.; Lupi, S.M.; Giarratana, N.; Bloise, N.; Benedetti, L.; De Angelis, M.G.C.; Baena, R.R.Y. Evaluation of Poly(Lactic-co-glycolic) Acid Alone or in Combination with Hydroxyapatite on Human-Periosteal Cells Bone Differentiation and in Sinus Lift Treatment. *Molecules* **2017**, *22*, 2109. [CrossRef] [PubMed]
39. Marcarelli, M.; Zappia, M.; Rissolio, L.; Baroni, C.; Astarita, C.; Trovato, L.; Graziano, A. Cartilage Micrografts as a Novel Non-Invasive and Non-Arthroscopic Autograft Procedure for Knee Chondropathy: Three-Year Follow-Up Study. *J. Clin. Med.* **2021**, *10*, 322. [CrossRef]
40. Marcarelli, M.; Fiammengo, M.; Trovato, L.; Lancione, V.; Novarese, E.; Indelli, P.F.; Risitano, S. Autologous Grafts in the Treatment of Avascular Osteonecrosis of the Femoral Head. 1885. Available online: https://www.actabiomedica.it (accessed on 1 June 2023).
41. Hawwam, S.A.; Ismail, M.; Elhawary, E.E. The role of autologous micrografts injection from the scalp tissue in the treatment of COVID-19 associated telogen effluvium: Clinical and trichoscopic evaluation. *Dermatol. Ther.* **2022**, *35*, e15545. [CrossRef]

42. Niimi, Y.; Baba, K.; Tsuchida, M.; Takeda, A. A Histological Evaluation of Artificial Dermal Scaffold Used in Micrograft Treatment: A Case Study of Micrograft and NPWT Performed on a Postoperative Ulcer Formation after Tumor Resection. *Medicina* **2022**, *58*, 73. [CrossRef]
43. Andreone, A.; De Hollander, D. Case Report A Case Report on the Effect of Micrografting in the Healing of Chronic and Complex Burn Wounds. *Int. J. Burn. Trauma* **2020**, *10*, 15–20.
44. Aliberti, F.; Paolin, E.; Benedetti, L.; Cusella, G.; Ceccarelli, G. 3D bioprinting and Rigenera®micrografting technology: A possible countermeasure for wound healing in spaceflight. *Front. Bioeng. Biotechnol.* **2022**, *10*, 937709. [CrossRef]
45. Nummi, A.; Mulari, S.; Stewart, J.A.; Kivistö, S.; Teittinen, K.; Nieminen, T.; Lampinen, M.; Pätilä, T.; Sintonen, H.; Juvonen, T.; et al. Epicardial Transplantation of Autologous Cardiac Micrografts During Coronary Artery Bypass Surgery. *Front. Cardiovasc. Med.* **2021**, *8*, 726889. [CrossRef] [PubMed]
46. Trovato, L.; Monti, M.; del Fante, C.; Cervio, M.; Lampinen, M.; Ambrosio, L.; Redi, C.A.; Perotti, C.; Kankuri, E.; Ambrosio, G.; et al. A New Medical Device Rigeneracons Allows to Obtain Viable Micro-Grafts From Mechanical Disaggregation of Human Tissues. *J. Cell. Physiol.* **2015**, *230*, 2299–2303. [CrossRef]
47. Blakytny, R.; Jude, E. The molecular biology of chronic wounds and delayed healing in diabetes. *Diabet. Med.* **2006**, *23*, 594–608. [CrossRef] [PubMed]
48. Yu, J.R.; Navarro, J.; Coburn, J.C.; Mahadik, B.; Molnar, J.; Holmes, J.H.; Nam, A.J.; Fisher, J.P. Current and Future Perspectives on Skin Tissue Engineering: Key Features of Biomedical Research, Translational Assessment, and Clinical Application. *Adv. Healthc. Mater.* **2019**, *8*, 1801471. [CrossRef] [PubMed]
49. Andreone, A.; Hollander, D.D. A Retrospective Study on the Use of Dermis Micrografts in Platelet-Rich Fibrin for the Resurfacing of Massive and Chronic Full-Thickness Burns. *Stem Cells Int.* **2019**, *2019*, 8636079. [CrossRef]
50. Gurtner, G.C.; Werner, S.; Barrandon, Y.; Longaker, M.T. Wound repair and regeneration. *Nature* **2008**, *453*, 314–321. [CrossRef] [PubMed]
51. Diegelmann, R.F.; Evans, M.C. Wound healing: An overview of acute, fibrotic and delayed healing. *Front. Biosci.* **2004**, *9*, 283–289. [CrossRef]
52. Idriss, H.T.; Naismith, J.H. TNF alpha and the TNF receptor superfamily: Structure-function relationship(s). *Microsc. Res. Tech.* **2000**, *50*, 184–195. [CrossRef]
53. Tu, C.; Lu, H.; Zhou, T.; Zhang, W.; Deng, L.; Cao, W.; Yang, Z.; Wang, Z.; Wu, X.; Ding, J.; et al. Promoting the healing of infected diabetic wound by an anti-bacterial and nano-enzyme-containing hydrogel with inflammation-suppressing, ROS-scavenging, oxygen and nitric oxide-generating properties. *Biomaterials* **2022**, *286*, 121597. [CrossRef]
54. Ouyang, W.; Rutz, S.; Crellin, N.K.; Valdez, P.A.; Hymowitz, S.G. Regulation and Functions of the IL-10 Family of Cytokines in Inflammation and Disease. *Annu. Rev. Immunol.* **2011**, *29*, 71–109. [CrossRef]
55. Franco, R.; Panayiotidis, M.I.; Cidlowski, J.A. Glutathione Depletion Is Necessary for Apoptosis in Lymphoid Cells Independent of Reactive Oxygen Species Formation. *J. Biol. Chem.* **2007**, *282*, 30452–30465. [CrossRef] [PubMed]
56. Dall'Ago, P.; Silva, V.O.K.; De Angelis, K.L.D.; Irigoyen, M.C.; Fazan, R., Jr.; Salgado, H.C. Reflex control of arterial pressure and heart rate in short-term streptozotocin diabetic rats. *Braz. J. Med. Biol. Res.* **2002**, *35*, 843–849. [CrossRef] [PubMed]
57. Oberholzer, M.; Östreicher, M.; Christen, H.; Brühlmann, M. Methods in quantitative image analysis. *Histochem. Cell Biol.* **1996**, *105*, 333–355. [CrossRef] [PubMed]
58. Bussolati, G.; Radulescu, R.T. Blocking Endogenous Peroxidases in Immunohistochemistry. *Appl. Immunohistochem. Mol. Morphol.* **2011**, *19*, 484. [CrossRef]
59. Ohkawa, H.; Ohishi, N.; Yagi, K. Assay for lipid peroxides in animal tissues by thiobarbituric acid reaction. *Anal. Biochem.* **1979**, *95*, 351–358. [CrossRef] [PubMed]
60. Sedlak, J.; Lindsay, R.H. Estimation of total, protein-bound, and nonprotein sulfhydryl groups in tissue with Ellman's reagent. *Anal. Biochem.* **1968**, *25*, 192–205. [CrossRef]
61. Buege, J.A.; Aust, S.D. Microsomal lipid peroxidation. *Methods Enzymol.* **1978**, *52*, 302–310. [CrossRef] [PubMed]
62. Mohammad, H.M.; El-Baz, A.A.; Mahmoud, O.M.; Khalil, S.; Atta, R.; Imbaby, S. Protective effects of evening primrose oil on behavioral activities, nigral microglia and histopathological changes in a rat model of rotenone-induced parkinsonism. *J. Chem. Neuroanat.* **2023**, *127*, 102206. [CrossRef] [PubMed]